Energy Materials

Supporting information for

Single-atomic-Ni electrocatalyst derived from phthalocyanine-modified MOF for convoying CO_2 intelligent utilization

San-Mei Wang [1, 2, 5], Xiaoshi Yuan [1, 2, 5], Shenghua Zhou [2], Xiaofang Li [2], Shu-Guo Han [2], Wenlie Lin[2], Lirong Zheng[4], Dong-Dong Ma [2,*], Qi-Long Zhu [2, 3,*]

[1] College of Chemistry, Fuzhou University, Fuzhou 350002, China

[2] State Key Laboratory of Structural Chemistry, Fujian Institute of Research on the Structure of Matter, Chinese Academy of Sciences (CAS), Fuzhou 350002, China

[3] School of Materials Science and Engineering, Zhejiang Sci-Tech University, Hangzhou 310018, China

[4] Beijing Synchrotron Radiation Facility, Institute of High Energy Physics, Chinese Academy of Sciences, Beijing 100049, China

[5] Fujian College, University of Chinese Academy of Sciences, Fuzhou 350002, China

*Correspondence to: Prof. Dong-Dong Ma and Prof. Qi-Long Zhu, State Key Laboratory of Structural Chemistry, Fujian Institute of Research on the Structure of Matter, Chinese Academy of Sciences (CAS), 155 Yangqiao Road West, Gulou District, Fuzhou 350002, China. E-mail: madong@fjirsm.ac.cn, qlzhu@fjirsm.ac.cn

1. Materials and reagents

Carbon fiber paper (CFP, Toray, TGP-H-060, 30% waterproof, Shanghai Hesen Electric Co., Ltd, China), 1,8-diazabicyclo-(5,4,0)-undec-7-ene (DBU) (99%, Aladdin, China), 4-nitrophthalonitrile (98%, Aladdin, China), nickel (II) acetate tetrahydrate (98%, Sinopharm Chemical Reagent, China), 2-methylimidazole (98%, Sinopharm Chemical Reagent, China), zinc nitrate hexahydrate (99%, Sinopharm Chemical Reagent, China), dimethyl sulfoxide-d_6 (Adamas, (D, 99.9%), TMS (0.03%), China), deuterium oxide (Adamas, (D, 99.9%), China), Nafion D-520 dispersion (5% w/w in water and 1-propanol, ≥ 1.00 meq/g exchange capacity, Alfa Aesar).

2. Instrumentation and characterizations

^{1}H NMR spectra were recorded on an ECZ600S 600 MHz spectrometer. UV-Vis spectra were recorded on a Lambda 365 spectrophotometer. The metal contents of the catalysts were analyzed using ICP-AES on Ultima 2. Powder X-ray diffraction (XRD) patterns were collected on a desktop X-ray diffractometer (Rigaku-Miniflex600) at 40 kV voltage and 15 mA current with Cu Kα radiation. Transmission electron microscope (TEM) and high-resolution TEM (HRTEM) characterizations were carried out on FEI Titan Themis 200 at 200 kV. Aberration-corrected high-angle annular dark-field scanning TEM (HAADF-STEM) measurements were performed on JEM-ARM300F high-resolution transmission electron microscope operated at 200 kV. Scanning electron microscopy (SEM) was characterized on a ZEISS Sigma 300 field-emission scan electron microscope. The X-ray photoelectron spectroscopy (XPS) data were collected on a Thermo Fisher ESCALAB 250Xi spectrometer, using C 1s (284.8 eV) as the reference line. Raman spectra were recorded on a Labram HR800 Renishaw inVia system (Horiba) by using a 325 nm laser. The Brunauer-Emmett-Teller (BET) specific surface areas and pore sizes of the samples were performed with N_2 adsorption/desorption isotherms at liquid nitrogen temperature using automatic volumetric adsorption equipment (Belsorp-max). The gas products were determined by the gas chromatograph (Agilent 7820A) equipped with a molecular sieve 5A and HayeSep Q 80/100 mesh with Ar (≥99.999%) flowing as a carrier gas.

3. Experimental procedures

Synthesis of 2MIM-CN_2 [S1]

2-Methylimidazole (328 mg, 4 mmol), anhydrous K_2CO_3 (829 mg, 6 mmol) and 4-nitrophthalonitrile (519 mg, 3 mmol) were added in dry N,N-dimethylformamide (DMF, 20 ml), and unceasingly stirred for 72 h. Then, the reaction mixture was poured into 150 ml of deionization water. And the obtained precipitate was collected, washed with deionization water. Yield: 64.2 %. ^{1}H NMR (Dimethyl sulfoxide(DMSO)-d_6), δ/ppm: 8.34 (s, 1H, Ar-H), 8.29–8.27 (d, 1H, Ar-H), 8.03–8.01 (d, 1H, Ar-H), 7.44 (s, 1H, Im-H), 6.95 (s, 1H, Im-H), 2.35 (s, 3H, -CH_3).

Synthesis of IM_4NiPc [S1]

2MIM-CN_2 (208 mg, 1.0 mmol), nickel (II) acetate tetrahydrate (75 mg, 0.3 mmol) and dried 1-pentanol (5 ml) were added and stirred at 120 °C for 30 min under Ar atmosphere. Then 0.5 ml of DBU was added and stirred at 140 °C for 12 h. After the mixture was cooled to room temperature, the black green product was precipitated and washed with n-hexane for several times. The dried crude product was dissolved in dichloromethane and purified by neutral aluminium oxide column chromatography using dichloromethane/methanol (v/v=4/1) as eluents to give a dark violet solid. Yield: 74.1 %. HRMS: Calcd for $C_{48}H_{32}N_{16}Ni$: 890.2349 (exact mass); Found: 891.2442 ($[M+H]^+$).

Synthesis of ZIF-8

2.3 g of 2-methylimidazole was dissolved in 30 mL of methanol under ultrasound for 5 min, which was subsequently added into 30 mL of methanol containing 1.04 g $Zn(NO_3)_2{\cdot}6H_2O$ under vigorous stirring. The obtained solution was stirred for another 24 h. The precipitate was collected by centrifugation and washed with methanol for several times and dried in vacuum at 70 °C for overnight.

4. Electrochemical measurements

All the electrochemical measurements were performed with a CHI760E electrochemical workstation (Shanghai Chen-Hua Instrument Corporation, China) at 25 °C in 0.5 M $KHCO_3$ electrolyte with an airtight electrochemical H-type cell (Gaossunion), in which the two compartments (50 mL) with 30 mL of electrolyte on each side were separated by an exchange membrane (Nafion®117). Before testing, the Nafion membrane was treated in 5% H_2O_2 solution, pure water, 1 M H_2SO_4 solution and pure water for 1 h, respectively. A CFP supported catalyst, saturated Ag/AgCl electrode and Pt net were served as the working electrode, reference

electrode and counter electrode, respectively.

Before the CO_2 reduction experiments, the electrolyte (0.5 M $KHCO_3$) was saturated by bubbling pure CO_2 (99.999%) at the flow rate of 20.0 mL min^{-1} (using Mass flow controller D07-7B) for 30 min. The gas products were continuously conveyed into the gas-sampling loop (250 μl) of a gas chromatograph (GC, Agilent 7820A) for analyzing the gas products using thermal conductivity detector (TCD) and flame ionization detector (FID). The GC calibration curves for H_2 and CO were fitted by five times with independent single point sampling. Liquid products were analyzed by quantitative NMR using deuterium oxide (D_2O) as an internal standard after CO_2 reduction electrolysis for 3600 s. Solvent presaturation technique was implemented to suppress the water peak. The working electrodes were cycled 20 times with the scan rate of 0.1 V s^{-1} over the potential range (–0.18 to –1.18 V vs. RHE) by cyclic voltammetry (CV) before other measurements. The electrolyte was stirred with magnetic stir bar (Length: 2.0 cm) at the speed of 1000 rpm. The linear sweep voltammetry (LSV) polarization curves were tested at the scan rate of 5.0 mV s^{-1}. Tafel plots were obtained from the extrapolation of the linear region of the plot of overpotentials versus current densities. Every CFP work electrode was performed i-t curve measurements from −0.48 to −0.98 V vs. RHE, continuously running it for 1800 s each potential. The electrochemical impedance spectroscopy (EIS) at potential −0.58 V vs. RHE from 100 KHz to 0.1 Hz with an amplitude of 5.0 mV. To estimate the ECSA, cyclic voltammograms (CV) were tested by measuring double-layer capacitance (C_{dl}) under the potential window of 0.02 to −0.08 V vs. RHE at the various scan rates from 5 to 25 mV s^{-1}. Potentials were measured vs. Ag/AgCl electrode, and the results were reported vs. reversible hydrogen electrode based on the Nernst equation: E (vs. RHE) = E (vs. Ag/AgCl) + 0.1989 V + 0.059 × pH. Each measurement was repeated three times in order to avoid any incidental error. All potentials were without iR corrected.

Calculation of faradaic efficiency

Faradaic efficiency was calculated as following [S2]:

$$FE_x(\%) = \frac{J_x}{J_{total}} = \frac{V_x \times N \times F}{J_{total}}$$

FE_x: Faradaic efficiency for x production, F: Faradaic constant = 96485 C mol^{-1}, V_x: The production rate of x, N: The number of electrons transferred for production formation, J_{total}: The recorded total current density, J_x: Partial current density for x

production, x: CO or H_2.

5. Supplementary figures and tables

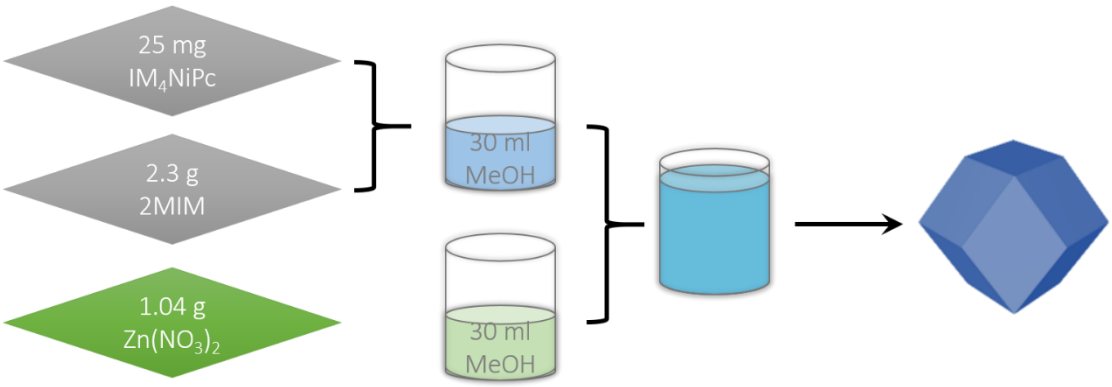

Supplementary Figure 1. Synthetic produce of ZIF-8-(IM_4NiPc).

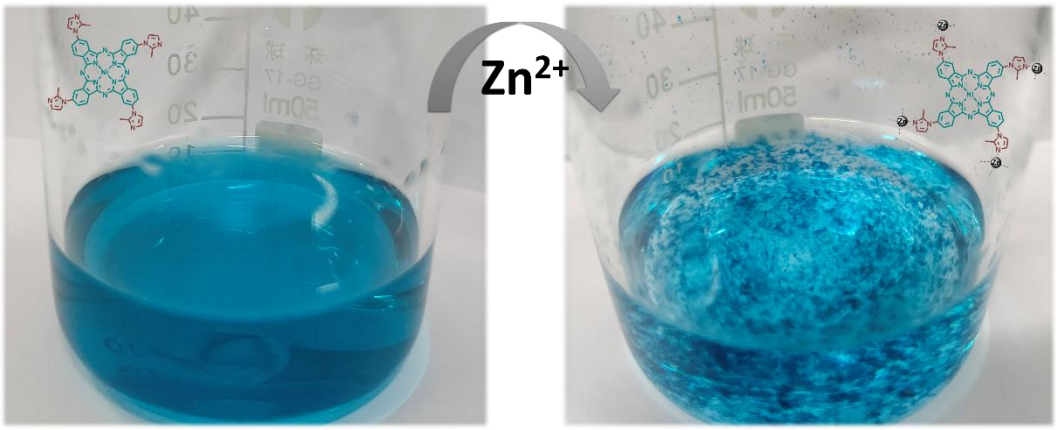

Supplementary Figure 2. Coordination interaction of IM_4NiPc with Zn^{2+}.

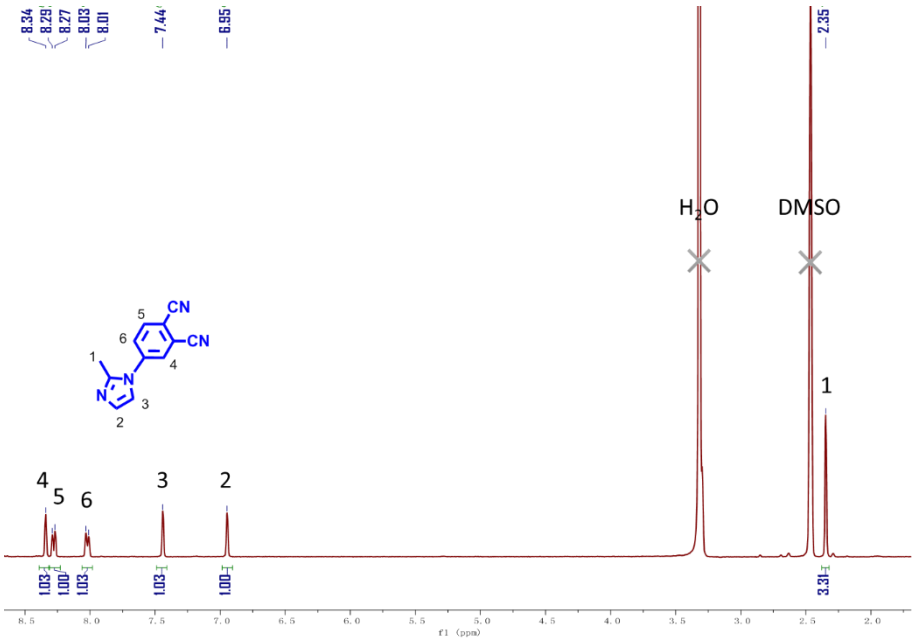

Supplementary Figure 3. ^1H NMR spectrum of 2MIM-CN_2 (400 MHz, DMSO-d^6).

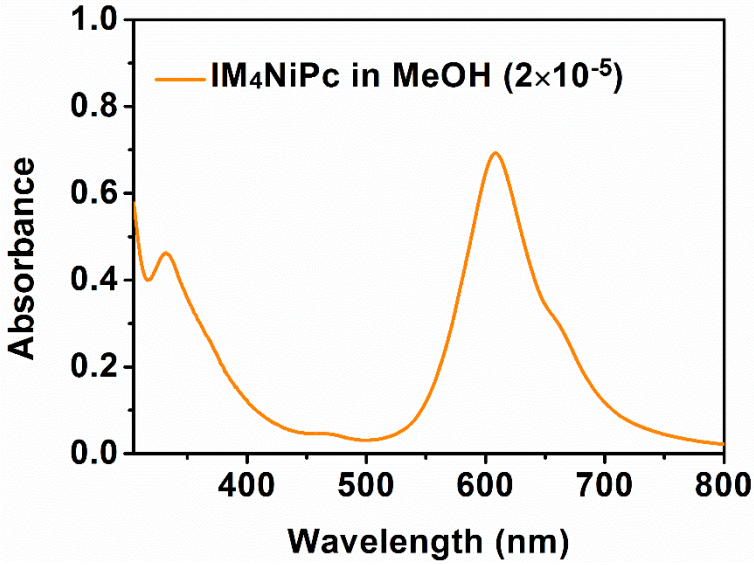

Supplementary Figure 4. UV-Vis spectrum of IM_4NiPc in MeOH.

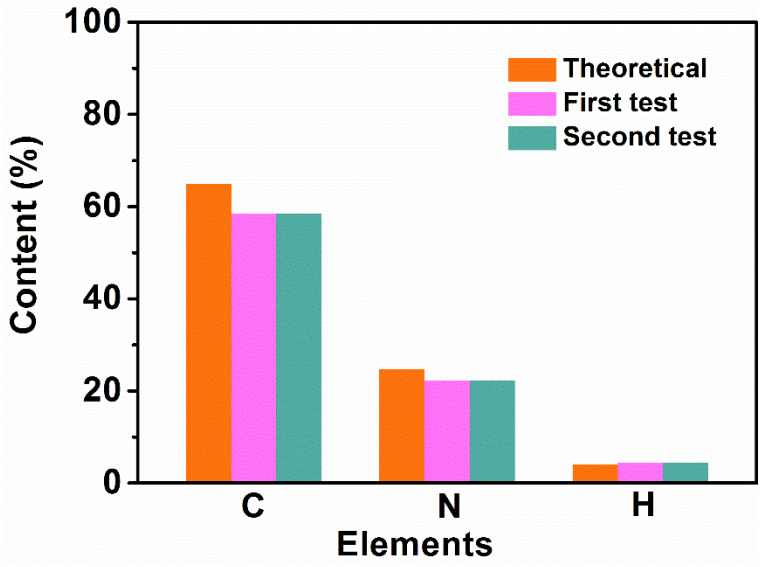

Supplementary Figure 5. Element analysis of IM_4NiPc.

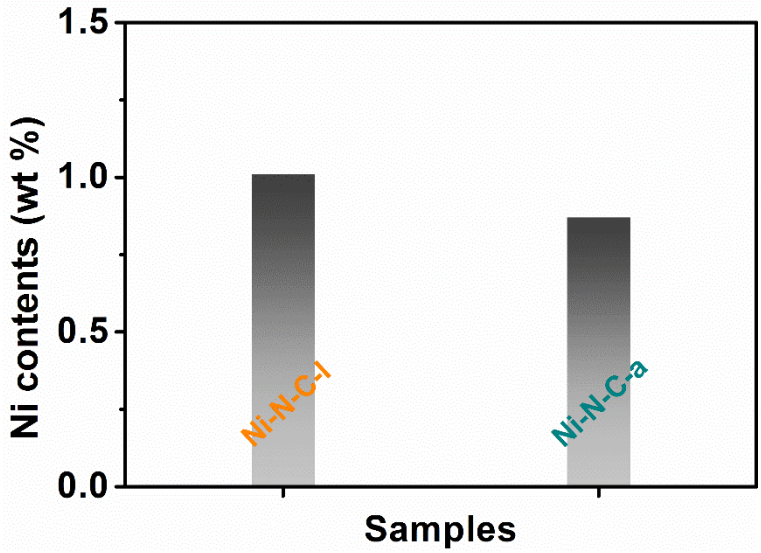

Supplementary Figure 6. Ni contents of Ni-N-C-l and Ni-N-C-a.

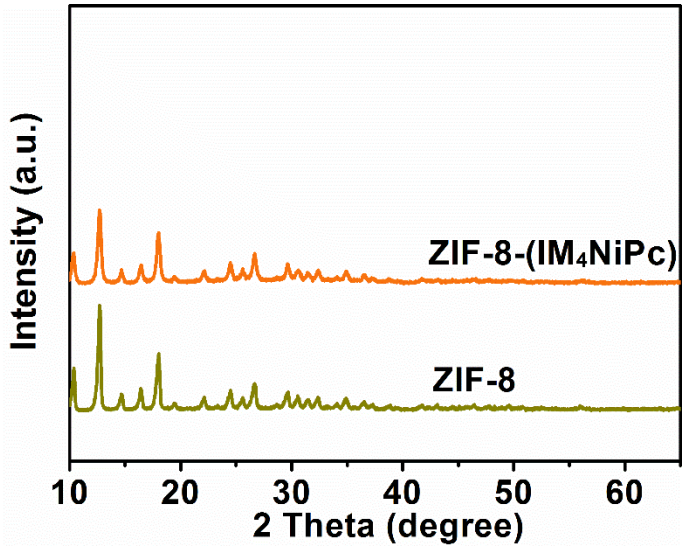

Supplementary Figure 7. PXRD patterns of ZIF-8 and ZIF-8-(IM_4NiPc).

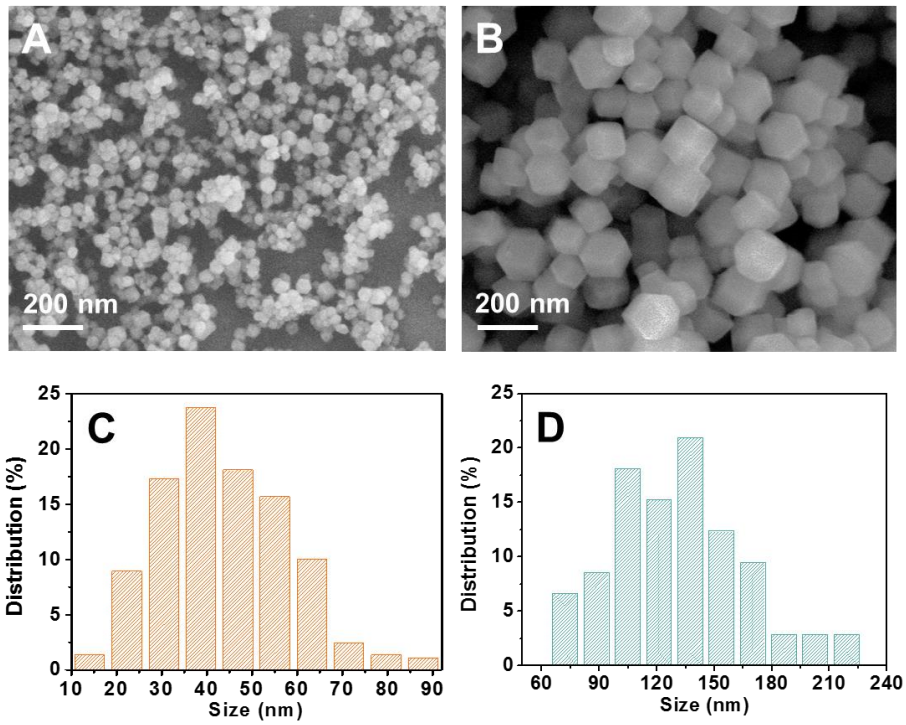

Supplementary Figure 8. SEM images of (A) ZIF-8-(IM_4NiPc) and (B) ZIF-8, diameter distribution of (C) ZIF-8-(IM_4NiPc) and (D) ZIF-8.

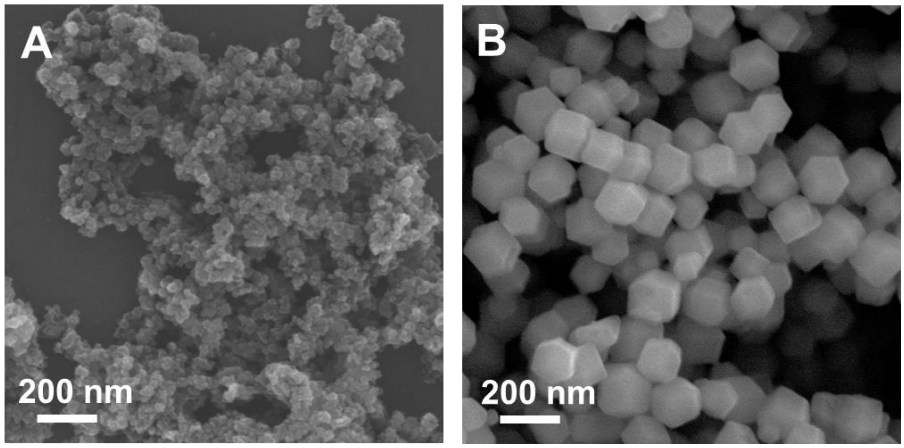

Supplementary Figure 9. SEM images of (A) Ni-N-C-l and (B) Ni-N-C-a.

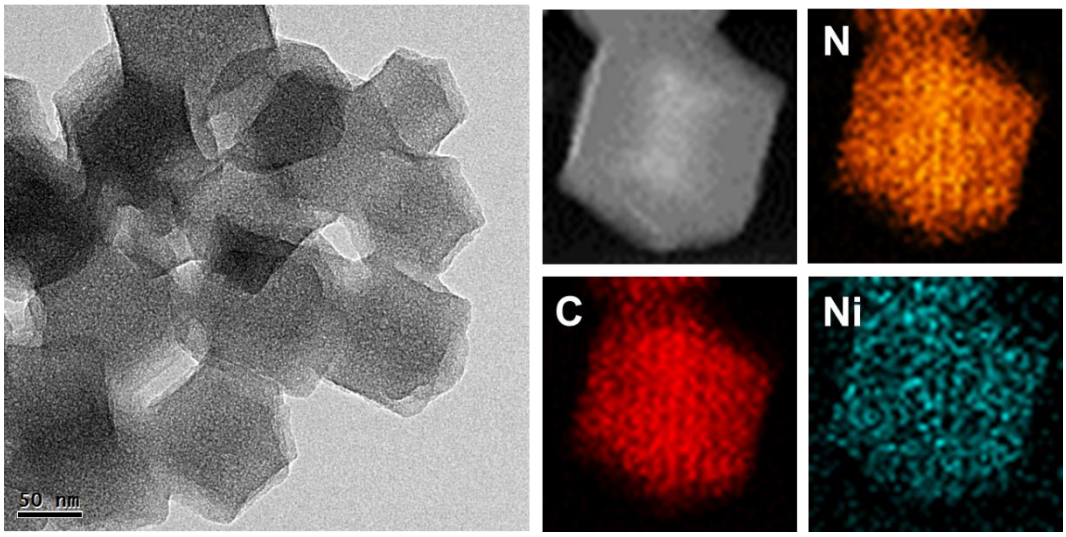

Supplementary Figure 10. TEM images of Ni-N-C-a.

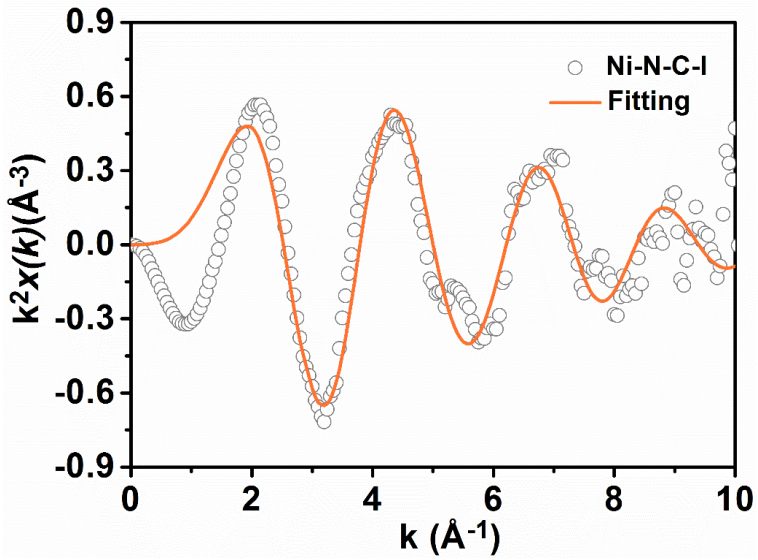

Supplementary Figure 11. FT-EXAFS R-space fitting curve of Ni-N-C-l.

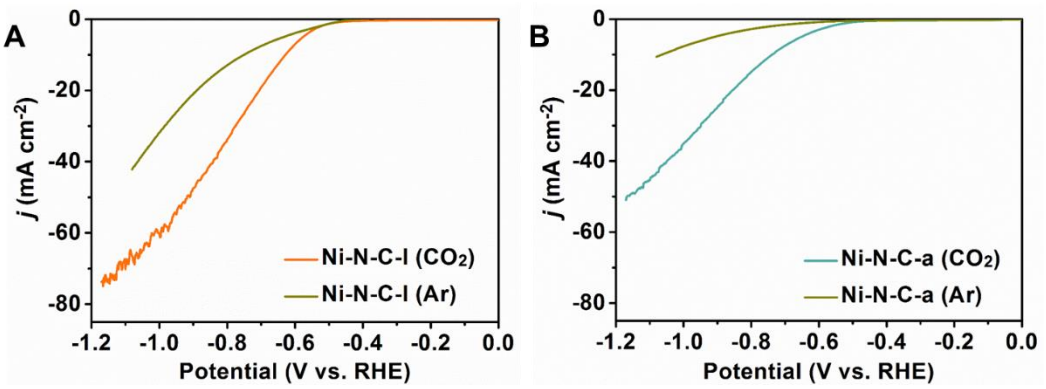

Supplementary Figure 12. LSV curves of (A) Ni-N-C-l and (B) Ni-N-C-a in CO_2 and Ar atmospheres.

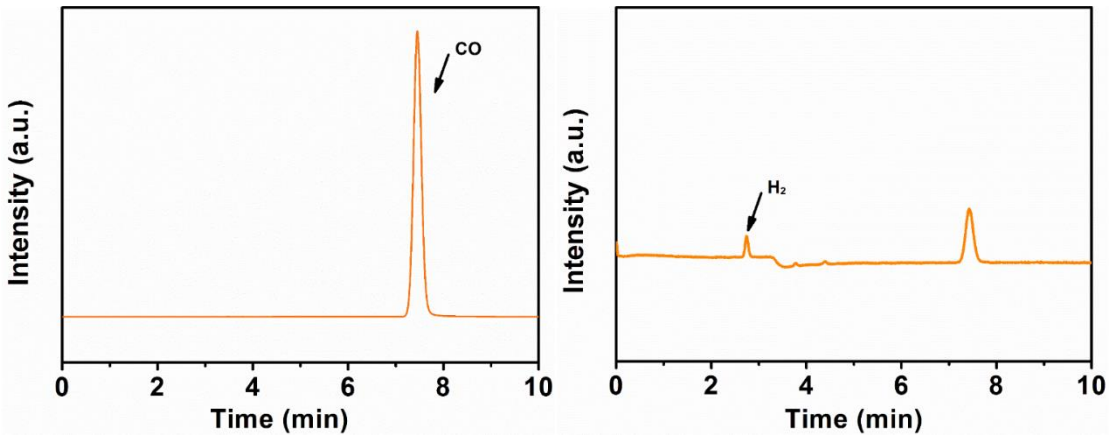

Supplementary Figure 13. Gas chromatography signal for gas-phase product analysis of Ni-N-C-l.

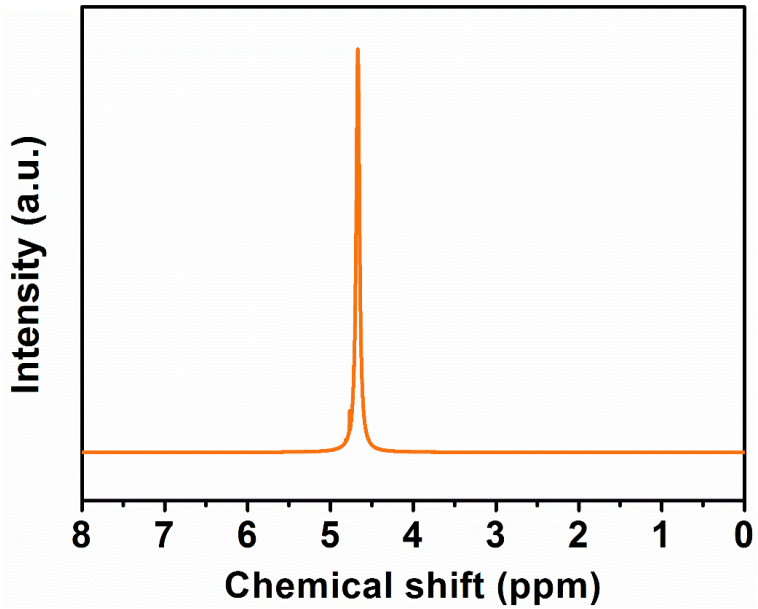

Supplementary Figure 14. ^{1}H NMR spectrum of electrolyte after test over Ni-N-C-l.

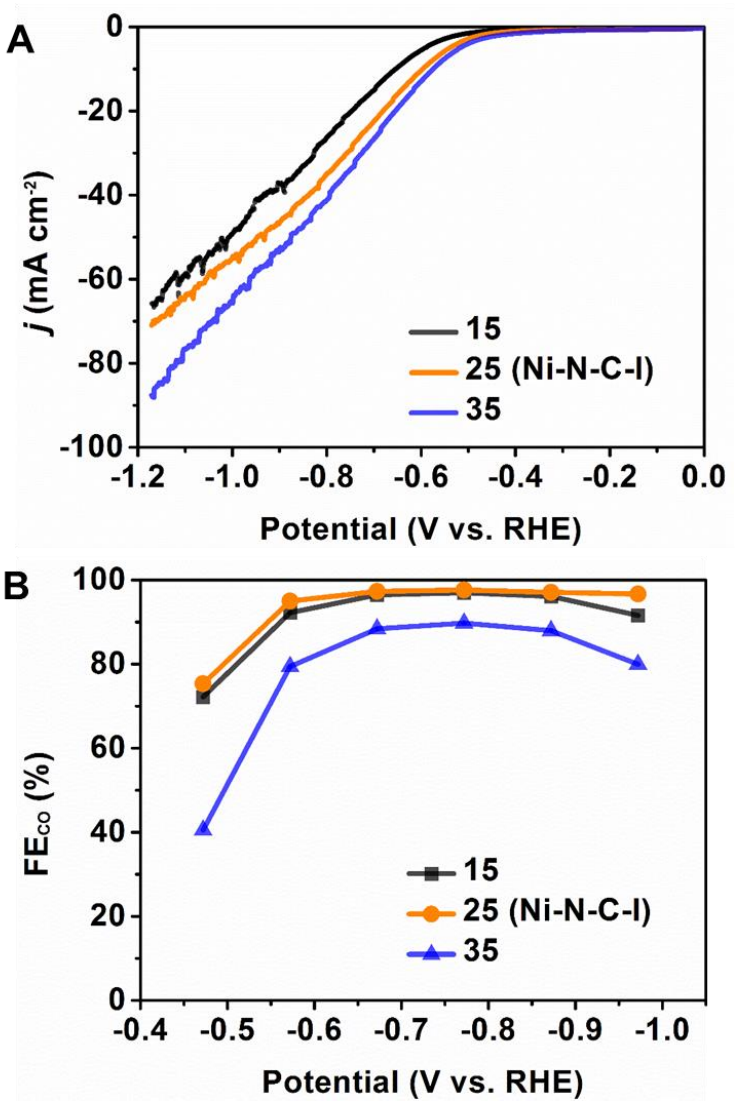

Supplementary Figure 15. Effect of IM_4NiPc amounts added during the catalyst preparation on eCO_2RR performance: (A) LSV curves and (B) FE_{CO}.

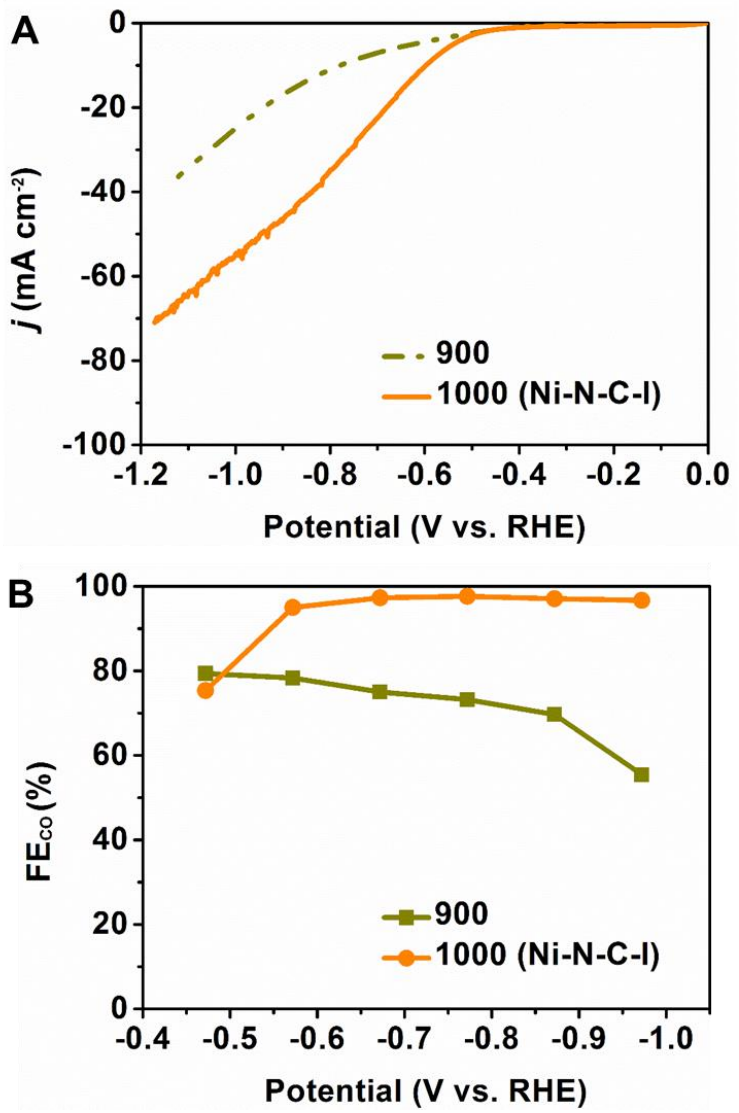

Supplementary Figure 16. Effect of carbonization temperatures during the catalyst preparation on eCO_2RR performance: (A) LSV curves and (B) FE_{CO}.

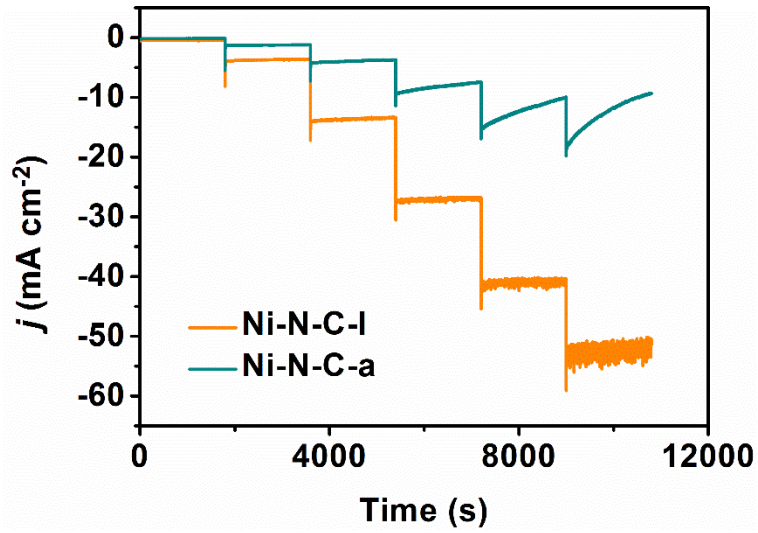

Supplementary Figure 17. Multipotential curves of Ni-N-C-l and Ni-N-C-a.

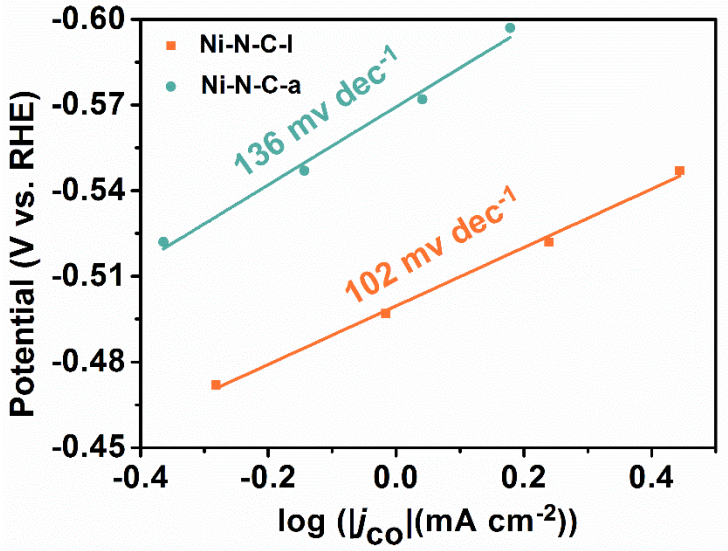

Supplementary Figure 18. Tafel slopes of Ni-N-C-l and Ni-N-C-a.

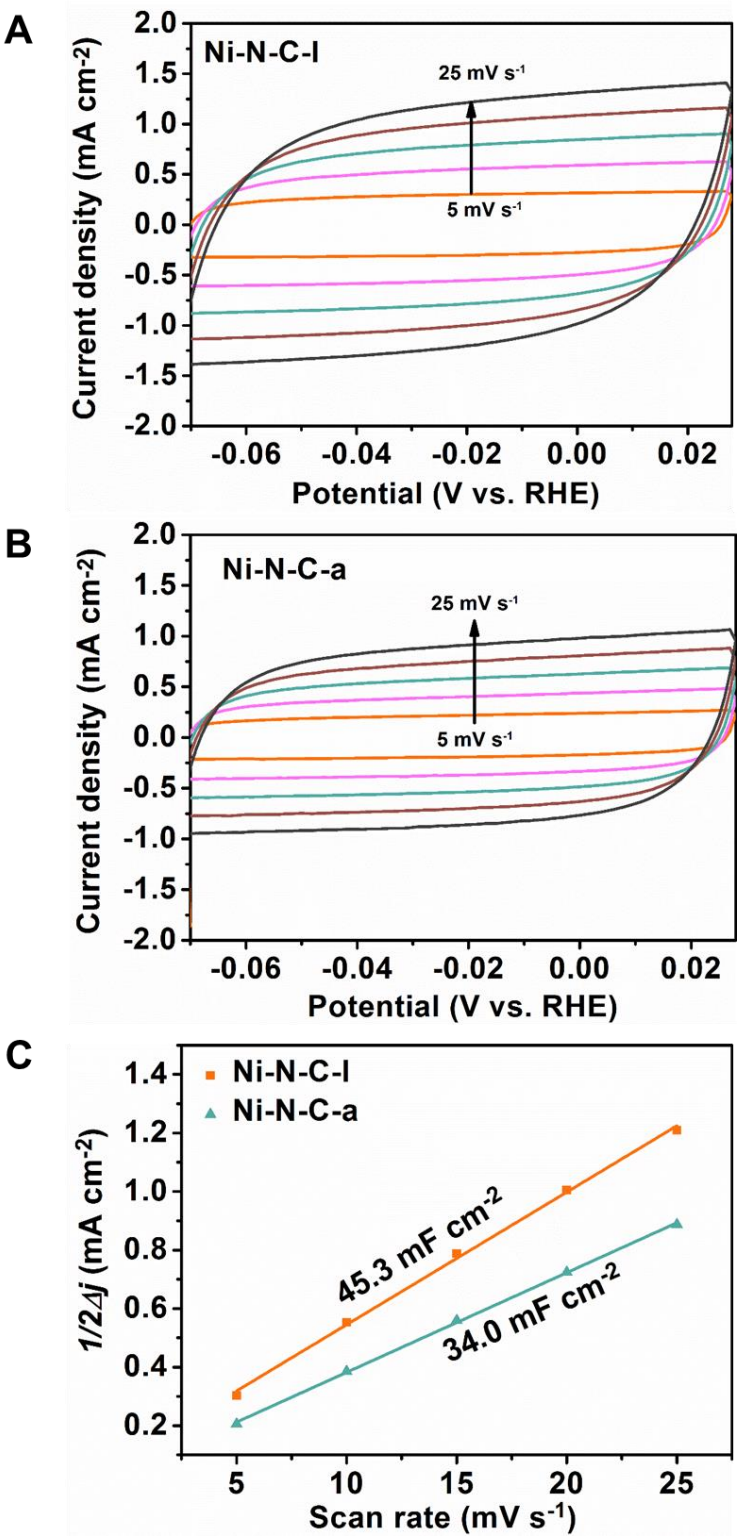

Supplementary Figure 19. (A,B) CV curves and (C) capacitance values of Ni-N-C-l and Ni-N-C-a.

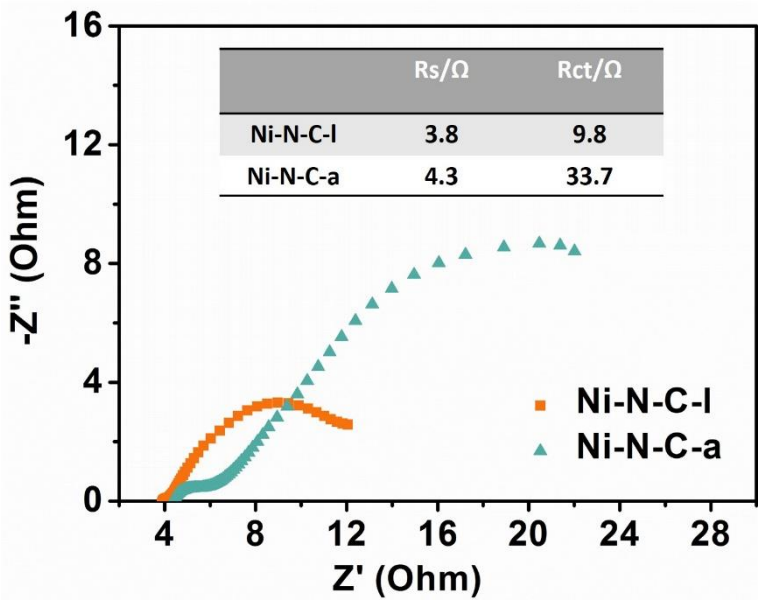

Supplementary Figure 20. Nyquist plots Ni-N-C-l and Ni-N-C-a.

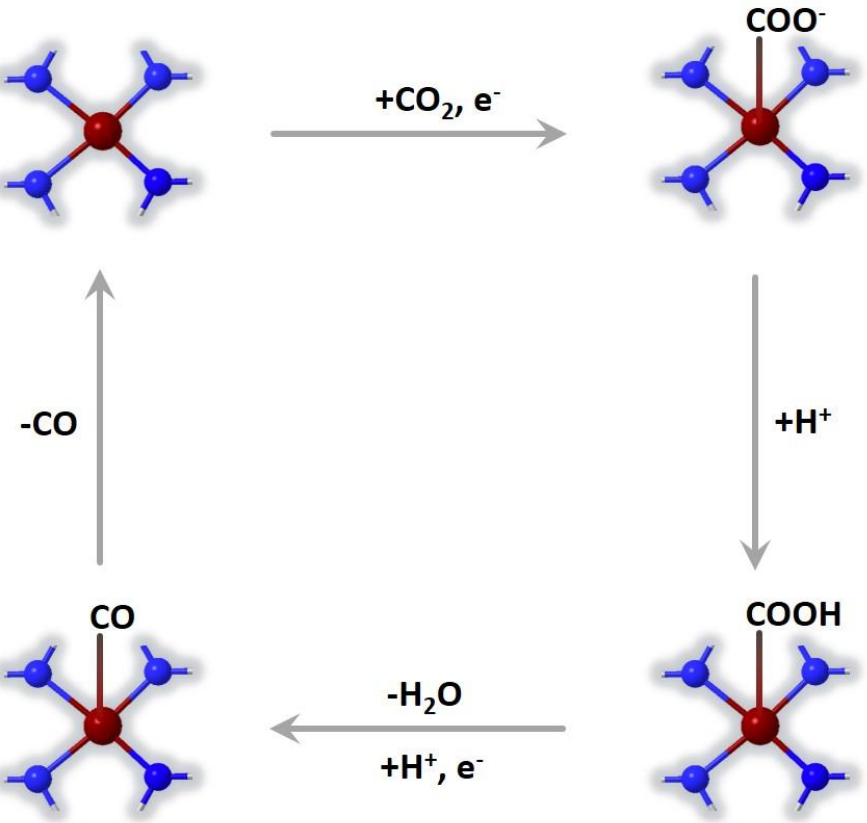

Supplementary Figure 21. Proposed reaction pathways of CO_2 electroreduction to CO.

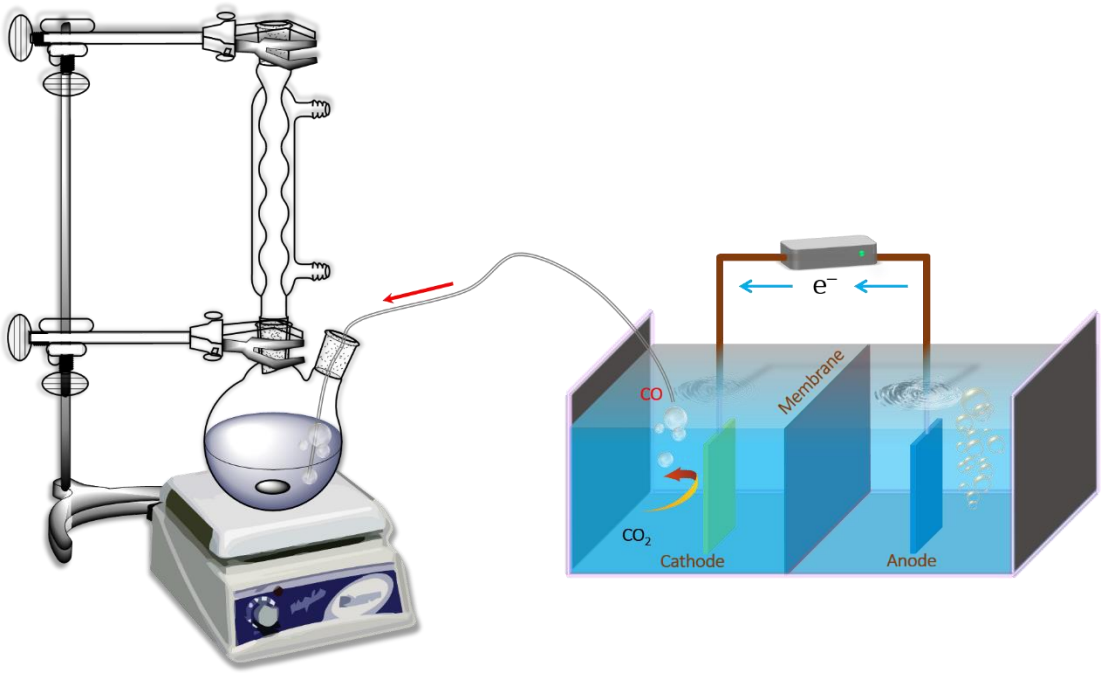

Supplementary Figure 22. Diagram of the electro/thermocatalytic cascade system for the synthesis of amide polymer materials.

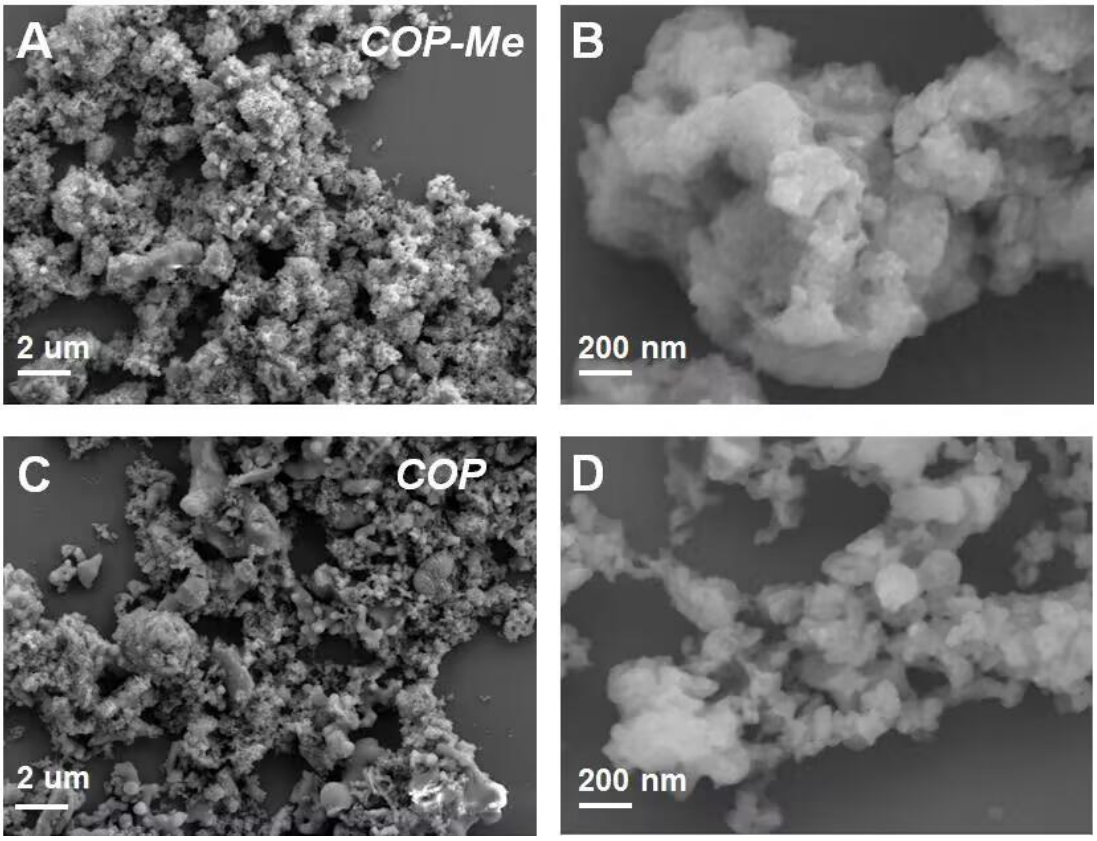

Supplementary Figure 23. SEM images of (A,B) COP-Me and (C,D) COP.

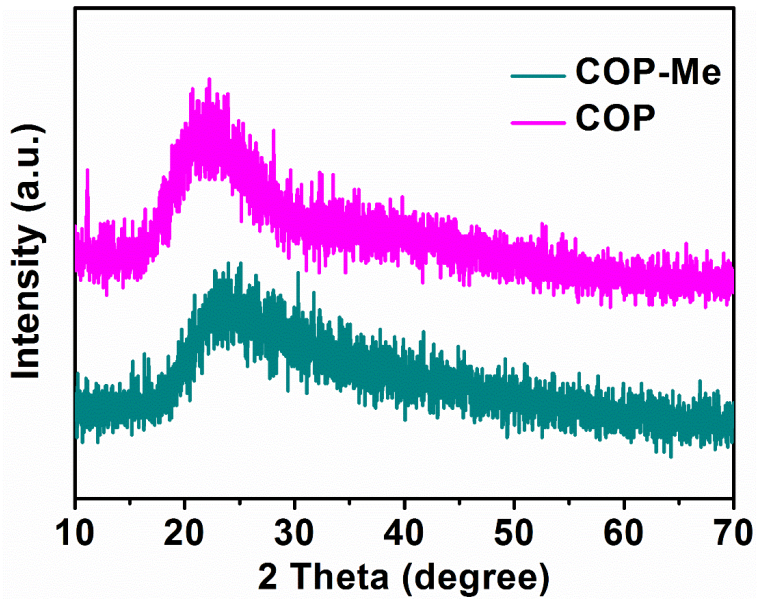

Supplementary Figure 24. PXRD patterns of COP-Me and COP.

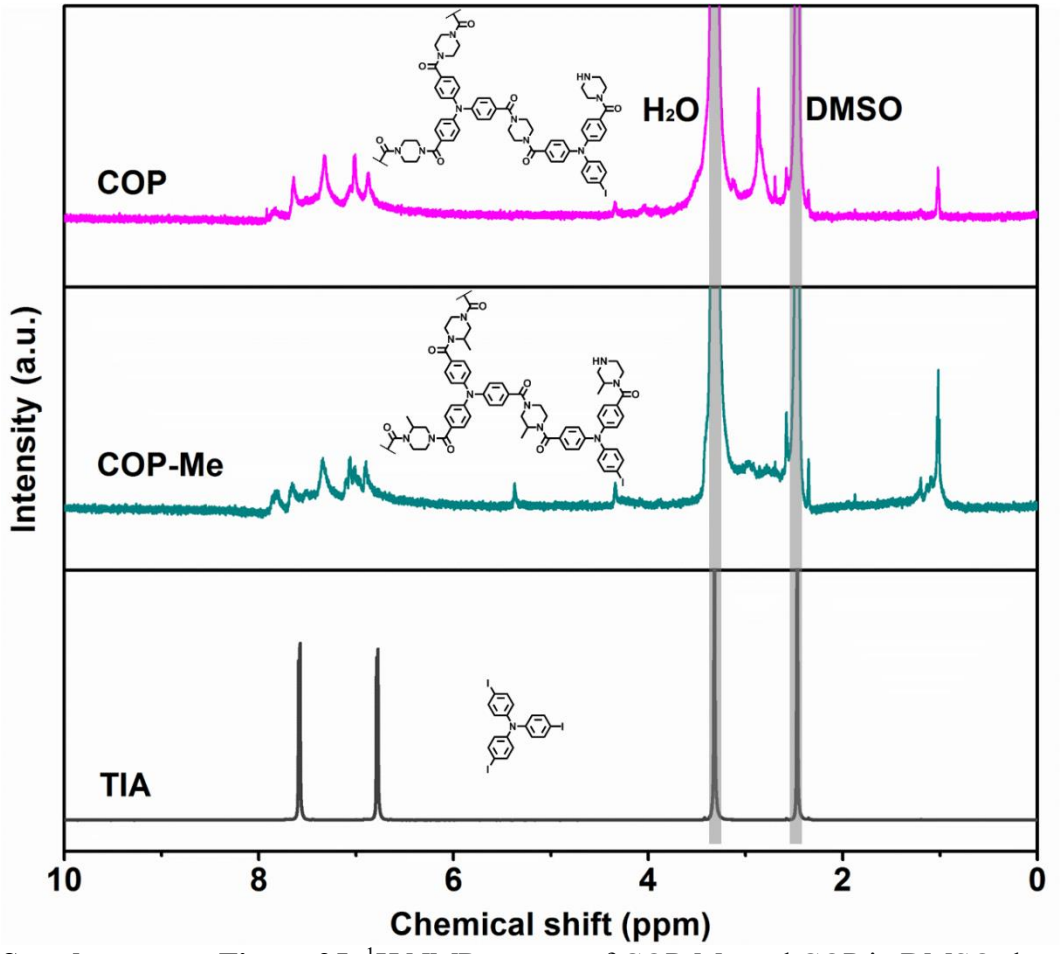

Supplementary Figure 25. ^{1}H NMR spectra of COP-Me and COP in DMSO-d_6.

Supplementary Table 1. Ni K-edge EXAFS data fitting results of Ni-N-C-l.

Sample	Scattering pair	CN	R (Å)	σ^2 (10^{-3} Å^2)	ΔE_0 (eV)	R factor
Ni-N-C-l	Ni-N	3.99	1.88	8	-6.21	0.03

σ^2 (10^{-3} Å^2) is the amplitude reduction factor;

CN is the coordination number;

R (Å) is interatomic distance (the bond length between central atoms and surrounding coordination atoms);

σ^2 is Debye-Waller factor (a measure of thermal and static disorder in absorber-scatterer distances);

ΔE_0 is edge-energy shift (the difference between the zero kinetic energy value of the sample and that of the theoretical model).

R factor is used to value the goodness of the fitting.

Supplementary Table 2. The eCO_2RR performances of the single-atom catalysts from recent literatures.

Catalysts	Electrolyte	Potential (V vs. RHE)	FEco	Refs.
Ni-N-C-l	0.5 M $KHCO_3$	–0.78	99%	This work
Ni-N_3-C	0.5 M $KHCO_3$	–0.65	95.6%	S3
Fe-N-C	0.1 M $KHCO_3$	–0.80	90%	S4
CoPc-COOH/CNT-NH_2	0.5 M $KHCO_3$	–0.88	90%	S5
Ni SAs/NC	0.5 M $KHCO_3$	–0.90	71.9%	S6
Ni-NG	0.1M $KHCO_3$	–0.58	95%	S7
NiN-GS	0.1 M $KHCO_3$	–0.68	93.2%	S8
Co-COF	0.5 M $KHCO_3$	–0.67	87%	S9
Sn/N-C	0.5 M $KHCO_3$	–0.60	91%	S10
Fe/NG	0.5 M $KHCO_3$	–0.60	80%	S11

6. References

S1. Ma D-D, Han S-G, Zhou S-H, Wei W-B, Li X, Chen B, Wu X-T, Zhu Q-L. Molecularly dispersed heterogenized metallomacrocycles: molecular structure sensitivity of CO_2 electrolysis. *CCS Chem* 2023; 5: 1827-40. [DOI:10.31635/ccschem.022.202202294]

S2. Ma D-D, Han S-G, Cao C, Li X, Wu X-T, Zhu Q-L. Remarkable electrocatalytic CO_2 reduction with ultrahigh CO/H_2 ratio over single-molecularly immobilized pyrrolidinonyl nickel phthalocyanine. *Appl Catal B Environ* 2020; 264: 118530. [DOI:10.1016/j.apcatb.2019.118530]

S3. Zhang Y, Jiao L, Yang W, Xie C, Jiang H-L. Rational fabrication of low-coordinate single-atom Ni electrocatalysts by MOFs for highly selective CO_2 reduction. *Angew Chem Int Ed* 2021; 60: 7607-11. [DOI:10.1002/anie.202016219]

S4. Mohd A N, Shan W, Hwang S, et al. Engineering atomically dispersed FeN_4 active sites for CO_2 electroreduction. *Angew Chem Int Ed* 2021; 60: 1022-32. [DOI:10.1002/anie.202012329]

S5. Xu H, Cai H, Cui L, Yu L, Gao R, Shi C. Molecular modulating of cobalt phthalocyanines on amino-functionalized carbon nanotubes for enhanced electrocatalytic CO_2 conversion. *Nano Res* 2023; 16: 3649-57. [DOI:10.1007/s12274-022-4578-x]

S6. Shen WJ. Ionic exchange of metal-organic frameworks to access single nickel sites for efficient electroreduction of CO_2. *Acta Phys-Chim Sin* 2018; 34: 113-4. [DOI:10.3866/PKU.WHXB201707101]

S7. Jiang K, Siahrostami S, Zheng T, et al. Isolated Ni single atoms in graphene nanosheets for high-performance CO_2 reduction. *Energy Environ Sci* 2018; 11: 893-903. [DOI:10.1039/C7EE03245E]

S8. Jiang K, Siahrostami S, Akey AJ, et al. Transition-metal single atoms in a graphene shell as active centers for highly efficient artificial photosynthesis. *Chem* 2017; 3: 950-60. [DOI:10.1016/j.chempr.2017.09.014]

S9. Diercks CS, Lin S, Kornienko N, et al. Reticular electronic tuning of porphyrin active sites in covalent organic frameworks for electrocatalytic carbon dioxide reduction. *J Am Chem Soc* 2018; 140: 1116-22. [DOI:10.1021/jacs.7b11940]

S10. Zhao Y, Liang J, Wang C, Ma J, Wallace GG. Tunable and efficient tin modified nitrogen-doped carbon nanofibers for electrochemical reduction of aqueous carbon dioxide. *Adv Energy Mater* 2018; 8: 1702524.

[DOI:10.1002/aenm.201702524]

S11. Zhang C, Yang S, Wu J, et al. Electrochemical CO_2 reduction with atomic iron-dispersed on nitrogen-doped graphene. *Adv Energy Mater* 2018; 8: 1703487. [DOI:10.1002/aenm.201703487]